GA–A27920

FAST ION TRANSPORT DURING APPLIED 3D MAGNETIC PERTURBATIONS ON DIII-D

by

M.A. VAN ZEELAND, N.M. FERRARO, W.W. HEIDBRINK, G.J. KRAMER, C.J. LASNIER, D.C. PACE, S.L. ALLEN, X. CHEN, T.E. EVANS, B.A. GRIERSON, M. GARCIA-MUNOZ, J.M. HANSON, M.J. LANCTOT, L.L. LAO, W.H. MEYER, R.A. MOYER, R. NAZIKIAN, D.M. ORLOV, C. PAZ-SOLDAN, J.-K. PARK and A. WINGEN

SEPTEMBER 2014

GENERAL ATOMICS

DISCLAIMER

GA–A27920

FAST ION TRANSPORT DURING APPLIED 3D MAGNETIC PERTURBATIONS ON DIII-D

by

M.A. VAN ZEELAND, N.M. FERRARO, W.W. HEIDBRINK,[1] G.J. KRAMER,[2] C.J. LASNIER,[3] D.C. PACE, S.L. ALLEN,[3] X. CHEN, T.E. EVANS, B.A. GRIERSON,[2] M. GARCIA-MUNOZ,[4] J.M. HANSON,[5] M.J. LANCTOT, L.L. LAO, W.H. MEYER,[3] R.A. MOYER,[6] R. NAZIKIAN,[2] D.M. ORLOV,[6] C. PAZ-SOLDAN, J.-K. PARK[2] and A. WINGEN[7]

This is a preprint of a paper to be presented at the Twenty-Fifth IAEA Fusion Energy Conf., October 13-18, 2014 in Saint Petersburg, Russia, to be published in the *Proceedings*.

[1]University of California Irvine, Irvine, California.
[2]Princeton Plasma Physics Laboratory, Princeton, New Jersey.
[3]Lawrence Livermore National Laboratory, Livermore, California.
[4]Max-Planck-Institut für Plasmaphysik, Garching, Germany.
[5]Columbia University, New York, New York.
[6]University of California San Diego, La Jolla, California.
[7]Oak Ridge National Laboratory, Oak Ridge, Tennessee.

Work supported in part by
the U.S. Department of Energy under
DE-FC02-04ER54698, SC-G903402, DE-AC02-09CH11466,
DE-AC52-07NA27344, DE-FG02-04ER54761,
DE-FG02-08ER54984 and DE-AC05-00OR22725

GENERAL ATOMICS PROJECT 30200
SEPTEMBER 2014

Fast Ion Transport During Applied 3D Magnetic Perturbations on DIII-D

EX/10-2

M.A. Van Zeeland[1], N.M. Ferraro[1], WW. Heidbrink[2], G.J. Kramer[3], C.J. Lasnier[4], D.C. Pace[1], S.L. Allen[4], X. Chen[1], T.E. Evans[1], B.A. Grierson[3], M. Garcia-Munoz[5], J.M. Hanson[6], M.J. Lanctot[1], L.L. Lao[1], W.H. Meyer[4], R.A. Moyer[7], R. Nazikian[3], D.M. Orlov[7], C. Paz-Soldan[1], J.K. Park[3] and A. Wingen[8]

[1]General Atomics, PO Box 85608, San Diego, CA 92186-5608, USA
[2]University of California at Irvine, Irvine, CA 92697, USA
[3]Princeton Plasma Physics Laboratory, PO Box 451, Princeton, NJ 08543-0451, USA
[4]Lawrence Livermore National Laboratory, 7000 East Ave, Livermore, CA 94550, USA
[5]Max-Planck-Institut für Plasmaphysik, Euratom Association, Garching, Germany.
[6]Columbia University, 116th St and Broadway, New York, NY 10027, USA
[7]University of California San Diego, 9500 Gilman Dr., La Jolla, CA 92093-0417, USA
[8]Oak Ridge National Laboratory, PO Box Oak Ridge, TN 37831, USA
email: vanzeeland@fusion.gat.com

Abstract. Pitch angle and energy resolved measurements show fast ion losses correlated with applied 3D fields in DIII-D plasmas. In DIII-D L-mode discharges with a slowly rotating n=2 magnetic perturbation, loss signals arising on separate scintillator detectors synchronized with the applied fields are observed to decay within one poloidal transit time after beam turn-off indicating they arise predominantly from prompt loss orbits. Full orbit following using M3D-C1 calculations of the perturbed fields and kinetic profiles reproduce many features of the measured losses and points to the importance of the applied 3D field phase with respect to the beam injection location in determining the overall impact on prompt beam ion loss. Modeling of these results includes a self-consistent calculation of the 3D perturbed beam ion birth profiles and scrape-off-layer ionization, a factor found to be essential to reproducing the experimental measurements. Extension of the simulations to full slowing down timescales, including fueling and the effects of drag and pitch angle scattering, show the applied n=3 resonant magnetic perturbations (RMPs) in edge localized mode (ELM) suppressed H-mode plasmas can induce a significant loss of energetic particles from the core. With the applied fields, up to 3.9% of the previously confined particles injected at full energy (~80 keV) are predicted to be lost before thermalization. These particles, originating from minor radii ρ>0.7, are predicted to be primarily lost to the divertor and outboard midplane region, consistent with wide field-of-view infrared periscope measurements of wall heating in n=3 RMP ELM suppressed plasmas. Edge fast ion D-alpha (FIDA) measurements also confirm a large change in edge FIDA emission due to the n=3 fields where the effect was isolated by using short 50ms RMP-off periods during which ELM suppression was maintained yet the fast ion profile was allowed to recover. The role of resonances between fast ion drift motion and the applied 3D fields in the context of selectively targeting regions of fast ion phase space is also discussed.

1. Introduction

In tokamaks, energetic particles (EPs) play critical roles in heating, current drive, momentum input and plasma stability, making their successful confinement essential. Due to their relatively collisionless orbits and long confined path lengths, EPs are particularly sensitive to toroidal symmetry-breaking fields which can cause EP transport and, potentially loss, the latter being a particular concern for device integrity. These non-axisymmetric fields can come from any number of sources, including fields either intrinsic to a given device (error fields or ripple), MHD induced, or imposed by external coil systems [1-4]. This work focuses on the low toroidal mode number (n=1–3) helical magnetic perturbations typically used for such things as edge-localized mode (ELM) or resistive wall mode (RWM) control. Similar coils have been predicted to cause 5% or more loss of neutral beam ions in ITER plasmas [5,6], making the accurate and validated modeling of this interaction a priority.

The DIII-D tokamak, is equipped with a set of six internal coils (I-coils) above and below the plasma midplane that are spaced uniformly in the toroidal direction and designed to make a radial field perturbation of up to ~120 G at the coil location immediately behind the first wall. These coils combined with two energy and pitch resolving fast ion loss detectors

(FILDs), an array of fast ion D-alpha (FIDA) views spaced across the plasma midplane, and wide field-of-view infrared imaging system are utilized to investigate the impact of 3D fields on the fast ion population. An example measurement (which will be discussed further in Sec. 3) showing fast ion loss clearly correlated with an applied n=2 field is shown in Fig. 1.

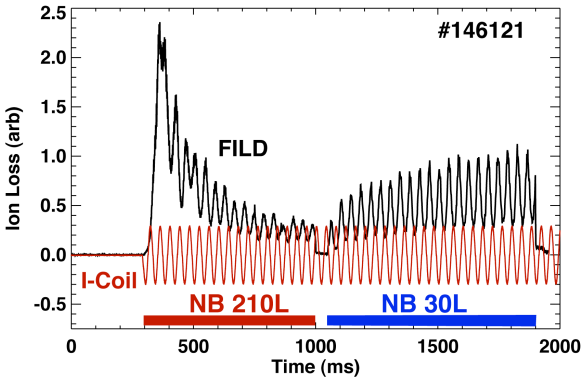

Fig. 1. Midplane FILD signal showing modulation of fast ion loss correlated with rotating n=2 field.

In this paper, we first discuss our modeling approach employed to address the issue of fast ion loss associated with 3D fields then move on to discuss two quite different plasma regimes and the experimental data showing fast ion loss in each regime along with comparisons to modeling for each case. Experimentally, the regimes presented are first, a DIII-D low-current, low beam power L-mode plasma in which the primary 3D field induced fast ion loss observed is a modulation of prompt beam ion loss. Following this, fast ion loss due to n=3 resonant magnetic perturbation (RMP) fields in an ELM suppressed H-mode plasma is discussed. In both cases, many important features of the measured losses are captured by modeling giving confidence in our ability to predict this important effect in DIII-D and future devices. Finally, a potentially positive aspect of applied 3D fields is discussed where it is pointed out that resonances between fast ion orbits and the applied fields exist in these discharges and could be used to selectively target specific regions of phase space.

2. Modeling Approach

The simulations presented in this paper combine full-orbit and beam deposition modeling with M3D-C1 [7] two-fluid resistive MHD calculations of the plasma response to non-axisymmetric magnetic field perturbations. The general workflow is described by the diagram in Fig. 2. Equilibrium and coil information from a single time in a discharge is used to calculate the plasma response to a single-n from a Fourier expansion of the applied 3D fields. The 3D perturbed density profile combined with equilibrium profiles is then used to calculate a beam ion birth profile. Particles from the beam ion birth profile are then followed in the M3D-C1 calculated non-axisymmetric magnetic fields. For simulations of the impact on prompt loss, orbits are followed for one or more bounce periods and particles are considered to hit the FILD detectors if they come within 5 cm of the detector slit. For long timescale simulations used to calculate the new confined EP profile, particles are introduced at a fixed rate and followed for slowing down timescales using the SPIRAL [8] code which includes the effects of Coulomb drag and pitch-angle scattering. In both types of simulations, particles are considered lost if their trajectory intersects a 3D model for the DIII-D inner wall. To simulate rotation of the 3D field, as in Fig. 1, the process is repeated with the M3D-C1 perturbed profiles rotated by the desired amount.

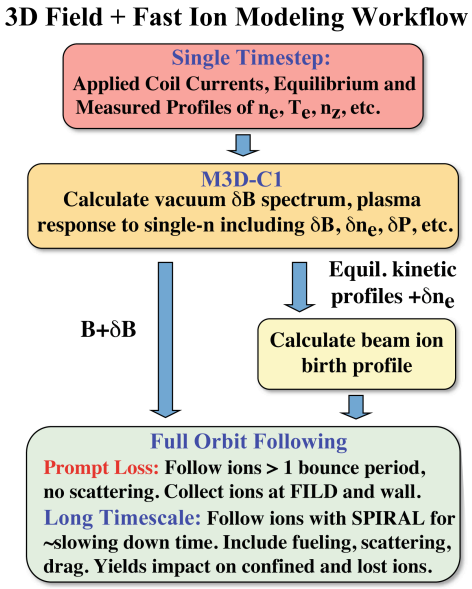

Fig. 2. Workflow for modeling impact of applied 3D fields on fast ion confinement in DIII-D.

The beam ion birth profile is calculated using a similar approach to that employed in NUBEAM [9] and FIDASIM [10]; this module, however, is unique in that it allows arbitrary 3D kinetic profiles such as those from M3D-C1 and naturally includes profiles outside the LCFS. Each beam is broken into several rays on which profiles of density, temperature, and

impurity density are interpolated. The attenuation for a given energy and species along each ray is calculated using ADAS beam stopping cross-sections [11] and from this attenuation profile, the probability for birth along a given ray is derived. A Monte Carlo selection process is used to first pick a ray from a given beam, then a position along the ray. An example full-energy birth profile for the 30L beam is shown in Fig. 3.

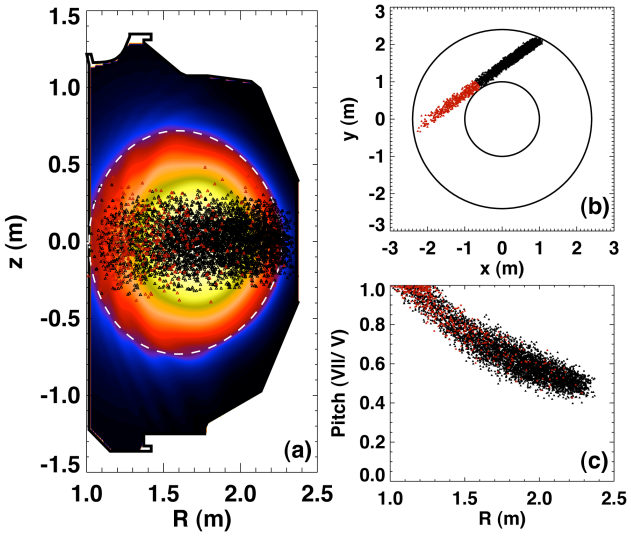

Fig. 3. Sample beam ion birth profile from n=2 L-mode experiments. (a) Birth profile overlaid on M3D-C1 calculated perturbed density profile. White dashed line is axisymmetric LCFS. (b) Top view. (c) Birth pitch distribution of particles.

3. 3D Field Impact on Prompt Beam Ion Loss, n=2 L-mode Discharge

In this experiment, a slowly rotating up/down symmetric (even parity) n=2 magnetic perturbation was applied to a low-elongation κ~1.16), low-current I_p= 0.6 MA) L-mode plasma with toroidal field B_T=2.0 T and normalized beta $\beta_N < 1$. The discharge was heated by two separate ~80 keV neutral deuterium beams, one co-current (30L) and the other counter-current (210L). L-mode plasmas were chosen to eliminate additional losses due to ELMs that could complicate analysis of imaging and spectroscopic data. Low elongation was used to make it easier for orbits to intersect the midplane FILD detector – with more elongated plasmas, EP losses typically intersect the outer wall well below the midplane FILD. The time history of the midplane FILD and a 25 Hz I-coil traveling waveform are shown in Fig. 1. The FILD signal clearly exhibits modulation of the fast ion losses at the I-coil waveform frequency along with several other features. The overall FILD signal is changing dramatically over the time window shown as a result of the beam timing, current penetration/q-profile evolution and density evolution [2]. During the first phase of the discharge, the plasma was heated predominantly by the counter-current beam injection (210L) with short blips of the 30L co-current beam for diagnostic purposes. At t = 1000 ms, there is a short period during which no beam heating is applied followed by constant injection of only the co-current beam.

The analysis in this paper focuses on the time period near t=1000 ms, an expansion of which is shown in Fig. 4. Before t = 1000 ms, when the 210L beam is being injected, loss to FILD is observed which terminates rapidly during the 50 ms Ohmic phase. After the Ohmic phase, the co-current 30L beam begins injection and loss is again observed to the midplane FILD, with a larger amplitude modulation. The fact that the losses decay almost immediately following turn-off of the 210L beam indicates that the losses are predominantly prompt in nature, i.e. beam neutrals are ionized and hit the FILD detectors within approximately one poloidal transit. In fact, if one zooms in further on the decay, the FILD signal is observed to decay in <20 microseconds after beam turn-off, whereas typical bounce periods are ~40 microseconds. Further evidence that the observed loss is prompt is the fact that small power oscillations in the 210L beam power at 36 Hz show up directly in the measured loss signals. If these signals were due to losses of beam ions that were previously confined or had experienced significant slowing down, these oscillations would be washed out. The fact that the

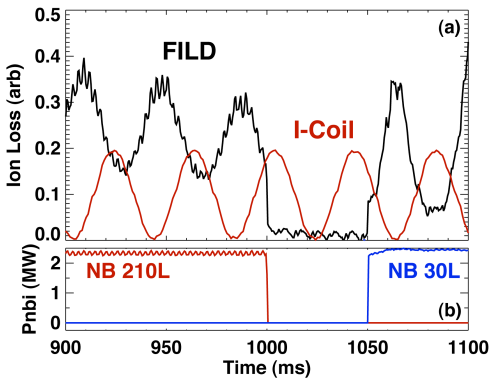

Fig. 4. Discharge 14612. Expanded region of Fig. 1. (a) FILD and I-coil time traces. (b) 210L and 30L neutral beam waveforms.

FILD signal is dominated by prompt beam ion loss is also consistent with the dependence of the FILD trace in Fig. 1 on the magnetic geometry. As the current penetrates, the beam ion confinement becomes better and the prompt loss decays significantly. During this time, however, the density is increasing, and the beam penetration becomes lower causing a shift in the beam deposition to larger which increases the relative prompt loss to the midplane FILD from the 30L beam.

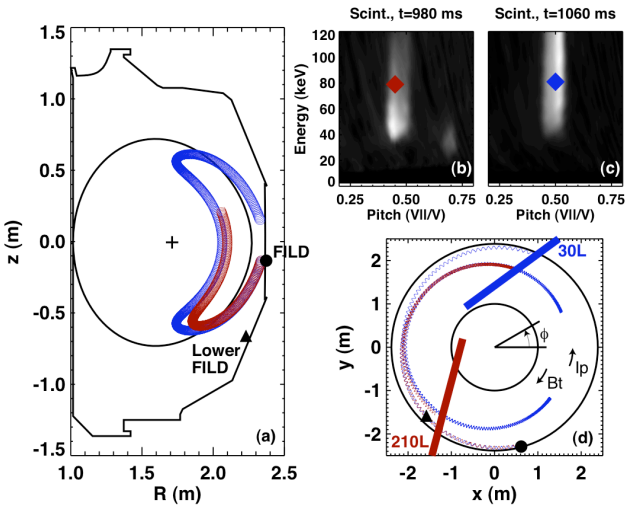

Fig. 5. (a) Reverse orbit following trajectories of ions with energy and pitch shown in panels (b) and (c). Red is from 210L beam, blue is 30L beam. (d) Top view.

Reverse orbit tracing of the unperturbed orbits from the FILD location combined with the measured velocity pitch angles can be used to find the approximate birth location and trajectories of the observed ions. The orbit-following results and relevant scintillator images are given in Fig. 5. From inspection of the scintillator images, the losses appear to include full-energy (~80 keV) beam ions from the 210L and 30L beams with the measured pitch of $v_{||}/v$=0.45 and $v_{||}/v$=0.5 respectively These orbits were followed backward in time until they overlapped with the corresponding beam. From Fig. 5(a), it is clear that counter beam ions promptly lost to FILD-mid in an unperturbed equilibrium must be born inside the LCFS near mid-radius and co-going beam ions are born outside the LCFS. Thus, to properly model FILD measurements of co-going beam ions in these discharges, beam ionization in the scrape-off-layer (SOL) must be taken into account.

To simulate this experiment, the prompt loss to FILD was calculated for ten different phases of the *n*=2 perturbation with 250,000 particles followed at each phase. As mentioned in the previous section, particles that come within 5 cm of FILD were considered to have hit the detector. To compare the experimental data directly to simulation, the midplane FILD data are mapped from time to the equivalent phase of the *n*=2 perturbation used in the simulations and scaled by the average FILD signal over one cycle – the results of which are shown in Fig. 6. The modeling results in Fig. 6(b) include both the perturbed birth profile and *n*=2 magnetic field with plasma response. Modeling captures many of the features apparent in the FILD data: larger modulation of 30L losses as compared to 210L, 30L losses peak near *n2 phase*=0, and an approximate 30 Deg phase shift between 30L and 210L loss modulation is also observed as in experiment. The depth of modulation from simulation, however, is smaller than that observed experimentally. There are several potential reasons for this disagreement, the first being that the modeling includes only the *n=2* contribution to the perturbed magnetic fields. Due to the finite number of coils in each row (six) there is a significant *n*=4 contribution that, in vacuum, can be up to half the amplitude of the *n*=2 fields. Another factor that can contribute to the difference is that the FILD-mid data include losses from full, half, and third energy components whereas modeling has been carried out only for the full energy component of the losses. While the results in Fig. 6 show a local increase/decrease in

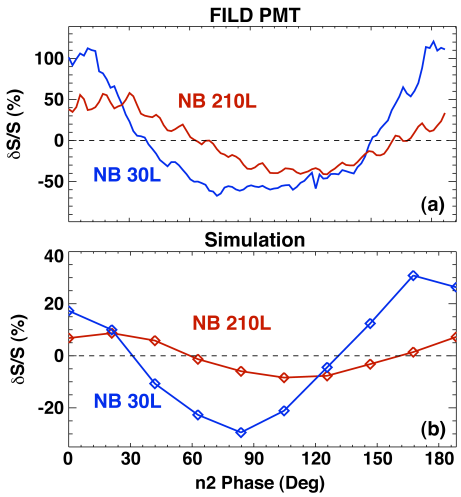

Fig. 6. DIII-D discharge 146121. (a) FILD PMT data from 30L (blue) and 210L (red) mapped to equivalent phase of the *n*=2 perturbation. Data from 40 ms interval centered at t = 965 ms and t = 1070 ms for the 210L and 30L beams respectively. Data are expressed as the difference from the mean (δS), divided by the mean (S) over the 40 ms interval.

prompt loss at the FILD detector about the mean, the simulations actually point to an overall increase in prompt loss due to the presence of the n=2 fields, with the level of increase dependent on the phase of the perturbation relative to the beam injection location.

4. 3D Field Induced Fast Ion Transport in n=3 RMP ELM Suppressed Plasmas

One of the primary motivations for the inclusion of 3D field coils in future tokamaks is the mitigation of ELMs [12]. In 2013, preliminary simulations of the expected fast ion transport in a typical DIII-D n=3 RMP ELM suppressed plasma were carried out. These simulations predicted a significant reduction in the edge fast ion profile due to the presence of the n=3 fields. In 2014, an experiment was carried out to investigate this effect. In the experiment, an ITER Similar Shape (ISS) [13] plasma was created with an odd-parity n=3 field, q_{95}=3.47, pedestal density $n_{e\text{-}ped} \sim 1.4\text{x}10^{19}$ cm^{-3}, and short 50 ms I-coil off periods to allow the fast ion profile to recover without loss of ELM suppression. Maintaining ELM suppression was a key part of this experiment since the ELMs themselves can cause significant edge fast ion transport as well as compromise FIDA measurements of the edge EP density by inducing large changes in the background. Time histories of the D-alpha emission, line-averaged density, and I-coil current are given in Fig. 7, along with the FIDA beam waveform. After density pumpout, ELM suppression is obtained near t = 2800 ms and maintained throughout each of the short I-coil off periods. During each off-period, the density begins to rise as expected but the pedestal remains below the threshold for ELMs to return.

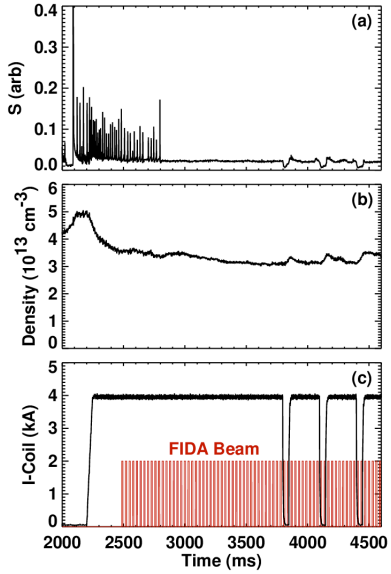

Fig. 7. DIII-D discharge 157545. Timetraces of (a) fast D-alpha photodiode. (b) Line-averaged density. (c) I-coil current (black), active beam for FIDA diagnosis (red).

FIDA measurements throughout the I-coil off periods show an increase in edge FIDA density then a return to lower levels after the *n=3* fields are switched back on. An example of the FIDA evolution throughout an n=3 off-pulse is shown in Fig. 8, where it is seen that the edge FIDA emission can increase by up to a factor of two or more during the n=3 off period, indicating a large change in the edge fast ion density.

In the same discharges, a wide field-of-view infrared periscope was used to measure the heating of the vessel first wall. Infrared periscope images show localized heating due to several fast ion related sources as well as a significant change in heat flux correlated with the I-coil off pulses. Heat flux images calculated from infrared camera measurements of the wall temperatures are shown before [Fig. 9(a)] and during [Fig. 9(b)] an n=3 off pulse. Three separate regions are highlighted in Fig. 9(a). These correspond to: 1) localized heating predominantly synchronized with the 210R counter current beam, a result of prompt beam ion loss, 2) heating of the center post due to 150R beam shine-through, 3) a large divertor heat flux that is reduced during the RMP off-phases.

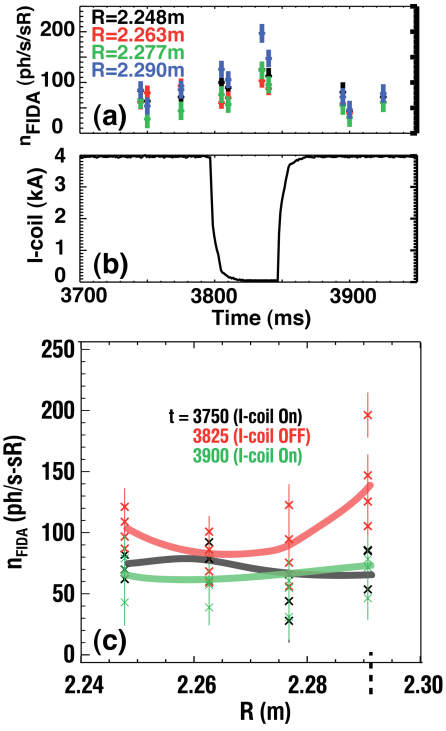

Fig. 8. #157545, edge FIDA data. (a) Time histories of FIDA density throughout n=3 off-period. (b) I-coil waveform. (c) FIDA density profiles before, during, after off-period. Dashed vertical line is axisymmetric LCFS.

Changes in divertor heat load due to loss of the thermal plasma during application of non-axisymmetric fields has been studied in this regime previously, where it was shown that particle drifts can play a large role in the resulting loss patterns [14]. Much of the divertor heat load was shown to be from thermal ion loss with higher energy ions reaching further from the calculated field line strike points. The same is certainly true for fast ion loss; it is expected that both will contribute to the divertor heat load and, in fact, the drift effects will be larger for fast ions.

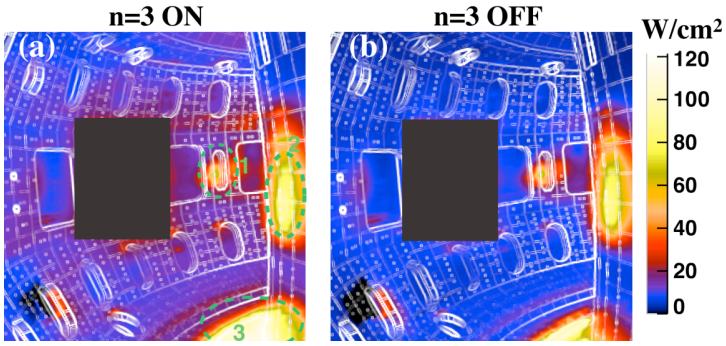

Fig. 9. Heat flux in #157418 calculated from infrared periscope measurements. (a) n=3 ON. Dashed green lines indicate: Region 1=primarily prompt loss from 210R counter beam. 2=Shine-through heating from 150R beam, 3=Divertor heat load. (b) n=3 off. Black rectangle indicates blocked view.

Full slowing-down timescale SPIRAL simulations of the n=3 induced fast ion transport have been carried out for discharge 157418. In the simulations, beam ions were injected at a constant rate over a 100 ms period. After a full slowing down steady state distribution was built up (~70 ms), n=3 fields were turned on. In Fig. 10(a), the loss rate of beam ions injected at the full energy normalized to the injection rate is shown vs. time (loss is defined as hitting the vessel wall before thermalization). When the n=3 fields are turned on at t=0, a large jump in losses occurs as previously confined particles are promptly lost. After approximately 7 ms, a new steady-state loss rate is reached that is roughly four times that of the case without *n=3* fields. With n=3 fields applied, roughly 13% of the injected full energy particles are lost before thermalization in the simulations. Figure 10(b) shows the confined fast ion profile at t = 23 ms in the simulations. From this figure, it is clear that the lost particles are coming from minor radii outside of ρ~0.7 (ρ = normalized square-root of toroidal flux), where the *n=3* fields are observed to induce up to a 65% deficit in the local confined fast ion profile (ρ~0.93) and a 3.9% reduction in the total number of confined fast ions. This is consistent with the large drop in FIDA density observed in Fig. 8, although detailed comparisons will require analysis with the FIDASIM code and SPIRAL simulations that evolve the edge density profile throughout the n=3 off phase.

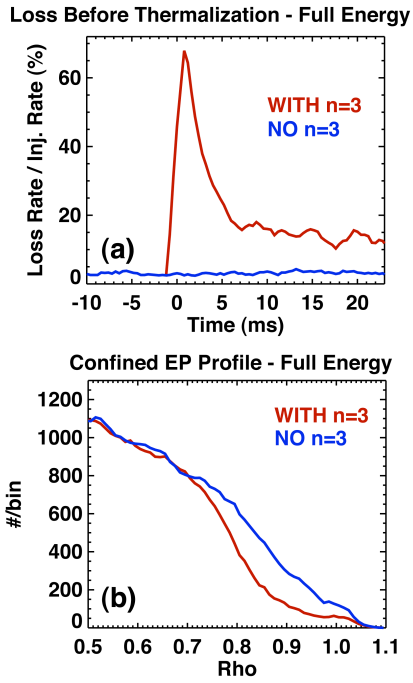

Fig. 10. SPIRAL simulations of 157418. (a) Loss rate before thermalization. n=3 is turned on at t = 0 ms. (b) Confined EP profile in simulations at t = 23 ms. Temporal and radial bins are 2 ms and 0.05 respectively.

SPIRAL simulations predict the position at which the lost particles strike the vessel wall, an example of which, remapped to the infrared camera field-of-view and overlaid with the vessel structure is shown in Fig. 11. Qualitatively, the regions of impact are similar to those observed with increased heat load. These calculations will eventually allow a direct comparison with the infrared periscope measurements from Fig. 9 as well as divertor infrared camera measurements, however, that will be presented in future work. Preliminary analysis shows the peak toroidally averaged fast ion heat flux due to loss of full energy injected beam ions occurs near the inner strike point and can be as large as ~100 W/cm^2 immediately following n=3 turn-on but drops to ~30 W/cm^2 after the initial burst of prompt losses.

Further details of the lost particles can be seen in Fig. 12, where the lost particles' birth (X) and final (◊) poloidal positions are shown. As can be seen from this figure, the majority of lost particles strike the wall in the divertor region, consistent with the location of the largest changes observed on the IR periscope. The losses shown in Fig. 12 are broken into four classes, those injected by the co- and counter-current beams and further divided by their birth location, on the high-field side (HFS) or low-field side (LFS) of the magnetic axis. Almost all beam ions born on the HFS of the magnetic axis are born onto passing orbits. Co-injected beam ions then travel counter-clockwise poloidally and end up near the inner leg of the separatrix. Counter-injected ions born on the HFS travel clockwise and end up primarily near the outer portion of the divertor. Not shown is the fact that these losses are primarily near the injection energy. Losses from the LFS of the magnetic axis are particles that are born onto primarily trapped orbits. These can span the divertor region when lost, but for co-injected particles, the losses are primarily concentrated in the outer portion of the divertor. Figure 12 also shows that a fraction of fast ions born at large radii are lost to the outer wall.

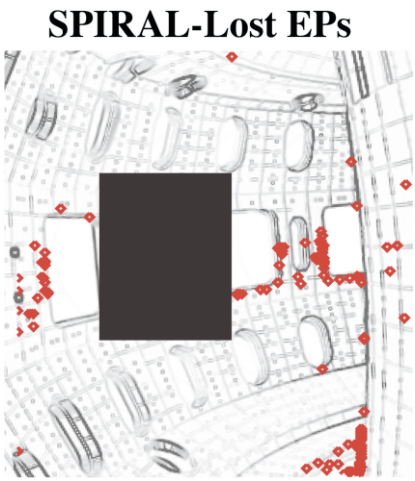

Fig. 11. Final location of lost particles injected at full energy. Locations remapped to infrared periscope field-of-view from Fig. 9.

The loss of particles born on the HFS of the magnetic axis leads one to believe much of the divertor heat load due to EP loss could be ameliorated by raising the central electron density. With low densities ($3.5\text{x}10^{13}$ cm^{-3}) such as in these RMP ELM suppressed plasmas, the beam penetration is larger and a significant fraction of particles are born at large minor radii on the HFS. Indeed, preliminary investigation of the heat load between ELMs before density pumpout is complete shows a reduction in divertor heat loads on the inner leg.

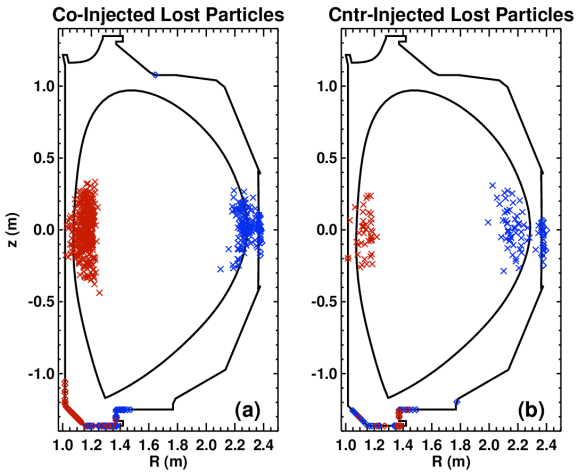

Fig. 12. Initial and final positions of lost particles due to n=3 RMP. (a) Co-current injected beam ions. (b) Counter-current injected beam ions. X = initial position, Diamond = final. Blue/red = HFS/LFS birth locations respectively.

5. Resonances Between Applied 3D Fields and Fast Ion Orbits

Interestingly, not all effects of symmetry-breaking fields on EPs are detrimental [15,16]. One recent experimental example shows applied $n=1$ perturbations could potentially be used as a means to alter EP-driven instabilities by interacting with the regions of phase space that are responsible for driving the modes [15]. A similar situation may be possible here where specific parts of phase space are targeted by taking advantage of resonances with applied 3D fields. It is well known that under certain conditions resonances between fast ion drift orbits and both static and dynamic non-axisymmetric fields can exist [16,17]. The standard condition for resonance is $\omega = n\omega_{prec} + l\omega_{bounce}$, where ω is the frequency of the perturbation, n is the toroidal mode number, ω_{prec} is the fast ion toroidal precession frequency, ω_{bounce} is the poloidal bounce frequency, and l is an integer. For zero frequency modes, the resonance condition is simply $l\omega_{bounce}/\omega_{prec} = n$. For low-$n$ perturbations such as those applied here, it is difficult for trapped thermal ions to fulfill this condition, while fast ions can. Shown in Fig. 13 is an example of the impact of resonance on the motion of a 45 keV ion that fulfills the n=2 resonance condition for the $n=2$ discharge discussed in Sec. 3. For reference, a 22 keV ion that does not fulfill the condition is also shown. For the particle at resonance, a much larger radial displacement is observed and, with collisions included, this region of phase space would experience larger transport. Figure 13(c) shows contours of the ratio of

$\omega_{bounce}/\omega_{prec}$ calculated for the particles launched along the outboard midplane with the pitch set by the direction of the 30L neutral beam with respect to the local magnetic field at that radius (the center of the pitch angle distribution generated by the beam). Note the radial electric field has been neglected here as it is a relatively small effect for this low-rotation discharge. The variation of this resonance with radius is a function of the local equilibrium and injection geometry so, by tailoring the current profile, toroidal field, beam, etc. the resonances could be placed wherever desired to target specific regions of phase space across the plasma or intentionally tailored to remove resonances and reduce EP transport.

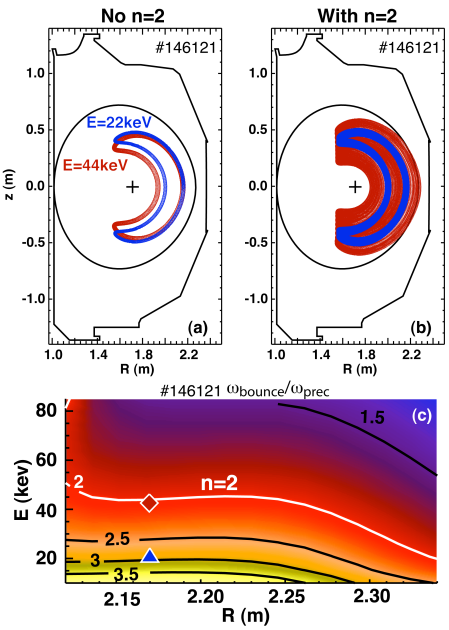

Fig. 13. (a) Unperturbed orbits in 146121. (b) Orbits with n=2 field applied at 5x expt. amplitude. 44 keV particle (red) fulfills resonance condition. (c) Ratio of $\omega_{bounce}/\omega_{prec}$ vs energy and radius for center of 30L beam. Initial conditions of 44 and 22 keV orbits in (a) and (b) overlaid as diamond and triangle.

6. Conclusions

Measurements and modeling of fast ion transport in DIII-D due to applied 3D magnetic field perturbations has been presented. In an L-mode discharge with a slowly rotating n=2 magnetic perturbation, the dominant observed signature is a modulation of prompt beam ion loss. Full orbit following combined with M3D-C1 calculations of the perturbed fields and kinetic profiles reproduces many features of the measured losses, particularly the phase and relative amplitude of the modulated loss from two different beams. Extension of the simulations to full slowing-down timescales, including fueling and the effects of drag and pitch angle scattering, show the applied n=3 RMPs in ELM suppressed H-mode plasmas can induce a significant loss of energetic particles from the core. With the applied fields, up to 3.9% of the previously confined injected particles injected at full energy (~80 keV) are predicted to be lost before thermalization. These particles, originating from minor radii ρ>0.7, are predicted to be primarily lost to the divertor and outboard midplane region, consistent with wide field-of-view infrared periscope measurements of wall heating in n=3 RMP ELM suppressed plasmas. Edge FIDA measurements also confirm a large change in edge FIDA emission due to the n=3 fields.

This material is based upon work supported in part by the U.S. Department of Energy, Office of Science, Office of Fusion Energy Sciences, using the DIII-D National Fusion Facility, a DOE Office of Science user facility, under Awards DE-FC02-04ER54698, SC-G903402, DE-AC02-09CH11466, DE-AC52-07NA27344, DE-FG0204ER54761, DE-FG02-07ER54917 and DE-AC05-00OR22725.

References

[1] SPONG D.A., Phys. Plasmas **18** (2011) 056109
[2] VAN ZEELAND M.A., et al., Plasma Phys. Control. Fusion **56** (2014) 015009
[3] M. Garcia-Munoz, et.al. Nucl. Fusion **53** (2013) 123008
[4] M. Garcia-Munoz, et.al., Plasma Phys. Control. Fusion **55** (2013) 124014
[5] SHINOHARA K., et al., Nucl. Fusion **51** (2011) 063028
[6] A. Snicker, E. Hirvijoki and T. Kurki-Suonio, Nucl. Fusion **53** (2013) 093028
[7] FERRARO N.M. and JARDIN S.C., J. Comput. Phys. **228** (2009) 7742
[8] KRAMER G.J., et al., Plasma Phys. Control. Fusion **55** (2013) 025013
[9] ALEXEI P., et al., Comput. Phys. Commun. **159** (2004) 3
[10] HEIDBRINK W.W., et al., Commun. Comput. Phys. **10** (2011) 716
[11] Atomic Data and Analysis Structure (ADAS) compilation. ADAS http://adas.phys.strath.ac.uk
[12] EVANS T.E., et al., Phys. Rev. Lett. **92** (2004) 235003
[13] EVANS T.E., et al., Nucl. Fusion **48** (2008) 024002
[14] WINGEN A., et al., Phys. Plasmas **21** (2014) 012509
[15] BORTOLON A., et al., Phys. Rev. Lett. **21** (2014) 265008
[16] MYNICK H.E., et al., Phys. Fluids B **5** (1993) 1471
[17] POLI E., et al., Phys. Plasmas **15** (2008) 032501